

# **FEM-Based Fatigue Endurance Evaluation of Engineering Components under Variable Amplitude Multiaxial Loading**

M. de Freitas, B. Li and J.L.T. Santos

Dept. of Mechanical Engineering, Instituto Superior Tecnico  
Av. Rovisco Pais 1, 1049-001 Lisboa, Portugal

## **ABSTRACT**

This paper presents an efficient approach for evaluating the high-cycle fatigue resistance of components under general multiaxial fatigue loading. The non-proportional loading effect is studied and a new efficient approach is proposed for evaluating the effective shear stress amplitude throughout a complex loading cycle. The idea of this approach is to construct a minimum circumscribed ellipse enclosing the loading path in the transformed deviatoric stress space. The new definition of the effective shear stress amplitude is the root mean square of the major semi-axis and the minor semi-axis of the minimum circumscribed ellipse, to take into account the out-of-phase loading effects. With this new approach, stress invariant-based multiaxial fatigue criteria, such as the Sines or Crossland criterion, can be applied with improved accuracy for fatigue evaluation under out-of-phase multiaxial loading. Test results collected from the literature, which include complex stress histories with different waveforms, frequencies, out-of-phase angles and mean stresses, were used to validate the approach here proposed. The methodology proposed in this paper can be implemented as a post-processing step using a commercial FEM code. A torque arm of an automotive rear suspension is used for illustration.

## **INTRODUCTION**

Engineering components are generally subjected to multiaxial fatigue loading, such as automobile suspension and transmission parts, blades in gas turbine rotors, pressure vessels, nuclear reactors and so on. It is one of the most difficult tasks in engineering design to translate the information gathered on the uniaxial fatigue tests to applications involving complex states of cyclic stress-strain conditions.

During the past decades, substantial research has been carried out to develop methods for multiaxial fatigue life prediction such as [1-6]. These methods differ considerably in formulation, in the range of applicability and in the reliability of the predictions. Most industrial applications involve high-cycle fatigue problems. For a comprehensive and updated review on high cycle metal fatigue see [7].

However, design engineers are often faced with difficulties in applying these approaches to multiaxial fatigue design of HCF components. One difficulty is that most of the existing multiaxial fatigue criteria can only provide good predictions for proportional (in-phase) loading. Another difficulty involves their

implementation for general complex multiaxial fatigue loading. In the pre-design stage and computer aided optimum design of components, efficient and easy-to-use methodologies are required for multiaxial crack initiation life prediction of components under general service loading.

Among current multiaxial fatigue criteria, stress invariant-based criteria, such as the Sines [8] and the Crossland [9] criterion, are attractive for engineering design of HCF components due to easy-to-use. They can provide good predictions for proportional loads with mean stress effects. However, they are not conservative for general complex multiaxial fatigue loading [10].

In this paper, non-proportional fatigue loading effects are considered and a new approach is proposed for evaluating the effective shear stress amplitude and mean value throughout a complex loading cycle. An efficient numerical algorithm is developed for implementing the proposed approach. Then, the Sines and Crossland criteria are extended to fatigue evaluation under general complex multiaxial loading. Finally, multiaxial fatigue test results collected from the literature, which include complex stress histories with different waveforms, frequencies, out-of-phase angles and mean stresses, are used for validating the developed approach. The proposed approach and the implemented procedure is illustrated through the example of a torque arm of an automotive rear suspension.

## **EFFECT OF NON-PROPORTIONAL MULTIAXIAL LOADING ON FATIGUE ENDURANCE**

General service loading of engineering components can be grouped in two categories: proportional and non-proportional loading. Proportional loading causes local stress states with fixed principal directions and constant ratios of the principal stresses fixed during the loading cycle. Non-proportional loading causes local stress states with principal directions and/or the ratios of the principal stresses varying with time during the loading cycle.

The effect of non-proportional multiaxial loading on the fatigue resistance of components has become an important topic of study. Although experimental results from non-proportional loading are limited, test results revealed the detrimental effect of non-proportional loading on fatigue endurance. For example, two typical load cases were tested by Heidenreich *et. al* [11]. In the first load case, an alternating normal stress  $\sigma_x$  occurs in combination with an alternating shear stress  $\sigma_{xy}$  with a phase shift of  $90^\circ$ , and in the second load case a pulsating normal stress  $\sigma_{xx}$  acts together with a compressive pulsating normal stress  $\sigma_{yy}$ . These two load cases have the same principal stress-time history [5]. In accordance with the classical multiaxial criteria, such as the von Mises criterion or the Tresca criterion, the same equivalent stresses are calculated in both load cases, which means that the same fatigue damage would be predicted by these classical multiaxial criteria. However, the fatigue damages caused by these two load cases are very different as verified by experiments [11].

The main difference between the two load cases is that load case 2 is proportional loading, whereas load case 1 is non-proportional loading due to the variation of the principal directions. In the transformed deviatoric stress space, the load path of case 1 becomes an ellipse due to the variation of the principal directions, whereas the load path of case 2 is a rectilinear line due to the unvaried principal direction [12]. This shows the necessity to consider carefully the non-proportional loading effect in the multiaxial fatigue design.

## **THE MINIMUM CIRCUMSCRIBED ELLIPSE APPROACH**

For multiaxial fatigue analysis, it is an essential and difficult task to evaluate the shear stress amplitude and mean value under complex multiaxial loading histories. There are three existing approaches [6]. They are the

longest projection, the longest chord and the minimum circumscribed circle methods as shown in Fig. 1, where  $\tau_{a1}$ ,  $\tau_{a2}$  and  $\tau_{a3}$  represent the shear stress amplitude obtained by these three methods respectively. A common weakness of these methods is that they can not differentiate the proportional and non-proportional loading paths.

A new approach, called the minimum circumscribed ellipse approach, is here proposed to account for the non-proportional loading effect. The idea is to construct a minimum circumscribed ellipse that can enclose the whole loading path throughout a loading block. The graphical representation of the new method and the relation with the minimum circumscribed circle approach [6] is illustrated in Fig. 2. Rather than defining  $\tau_a = R_a$  by the minimum circumscribed circle approach, a new definition of  $\tau_a = \sqrt{R_a^2 + R_b^2}$  is proposed [13-14], where  $R_a$  and  $R_b$  are the lengths of the major semi-axis and the minor semi-axis of the minimum circumscribed ellipse respectively. The important advantage of this new approach is that it can take into account the non-proportional loading effects in an easy way. As shown in Fig. 2, for the general non-proportional loading path 1, the shear stress amplitude is defined as  $\tau_a = \sqrt{R_a^2 + R_b^2}$ . For the rectilinear loading path 2, it is defined as  $\tau_a = R_a$ , since  $R_b$  is equal to zero for loading path 2 (in-phase loading case).

## IMPLEMENTATION OF THE MINIMUM CIRCUMSCRIBED ELLIPSE APPROACH

### *Synchronorous Sinusoidal Stress Histories*

If the local stress-time histories are synchronous sinusoidal waveforms, the corresponding loading path is an ellipse in the transformed deviatoric stress space. The minimum circumscribed ellipse is just the loading path curve. The lengths of the major semi-axis  $R_a$  and the minor semi-axis  $R_b$  can be solved analytically [12]. As an example, consider the load case with stress components expressed as:

$$\begin{aligned}\sigma_{xx} &= \sigma_{x,a} \sin(\omega t) + \sigma_{x,m} \\ \sigma_{yy} &= \sigma_{y,a} \sin(\omega t - \beta) + \sigma_{y,m} \\ \sigma_{xy} &= \sigma_{xy,a} \sin(\omega t - \gamma) + \sigma_{xy,m}\end{aligned}\quad (1)$$

The new definition of the shear stress amplitude in the transformed deviatoric stress space can be expressed in the analytical formulations:

$$\tau_a = \sqrt{R_a^2 + R_b^2} = \sqrt{\frac{\sigma_{x,a}^2 + \sigma_{y,a}^2 - \sigma_{x,a} \sigma_{y,a} \cos \beta}{3} + \sigma_{xy,a}^2 + \frac{\sigma_{y,a}^2 \sin^2 \beta}{4\sqrt{1+H^2}}}\quad (2)$$

where 
$$H = \frac{B+D}{A+C}\quad (3)$$

$$A = \frac{2\sigma_{x,a}^2 - 2\sigma_{x,a} \sigma_{y,a} \cos(\beta) + 0.5\sigma_{y,a}^2 \cos(2\beta)}{3}\quad (4)$$

$$B = \frac{2\sigma_{x,a} \sigma_{y,a} \sin(\beta) - \sigma_{y,a}^2 \sin(\beta) \cos(\beta)}{3}\quad (5)$$

$$C = 2\sigma_{xy,a}^2 \cos(2\gamma) + 0.5\sigma_{y,a}^2 \cos(2\beta)\quad (6)$$

$$D = 2\sigma_{xy,a}^2 \sin(2\gamma) + 0.5\sigma_{y,a}^2 \sin(2\beta)\quad (7)$$

### General Complex Stress Histories

For general irregular stress histories, it is a difficult problem to find the minimum circumscribed ellipse enclosing the whole loading path  $\psi'$  during a loading block, if solved by usual analytical methods. An efficient approach using the numerical mathematical programming method is developed to solve this problem [12-14]. To find the center point co-ordinates  $\mathbf{w}^*$ , the major semi-axis  $R_a$  and the minor semi-axis  $R_b$  of the minimum circumscribed ellipse (see Fig. 2), a sequential linear programming optimizer in conjunction with the simplex method [15] is employed efficiently. Then, the new definition of the shear stress amplitude can be calculated as  $\tau_a = \sqrt{R_a^2 + R_b^2}$ .

## A FEM-BASED PROCEDURE FOR MULTIAXIAL FATIGUE LIFE PREDICTION

The computation of the fatigue life of a component consists of two parts: dynamic stress computation and fatigue life prediction. Dynamic stress histories can be obtained either from experiment (mounting sensors or transducers on a physical component) or from simulation. The simulation-based approach consists of performing finite element analyses of the component using applied component loads. Then, the fatigue life prediction can be carried out as a post-processor.

The new approach for evaluating the effective shear stress amplitude throughout a loading cycle makes it possible to extend the Sines or the Crossland multiaxial fatigue criteria for finite fatigue life prediction under general multiaxial loading. After computing the local stress-time histories at critical component locations by the finite element method, the multiaxial fatigue evaluation procedure can be followed as:

### 1. Compute the Hydrostatic and Deviatoric Stresses

Split the stress tensor  $\boldsymbol{\sigma}(t)$  into its deviatoric and spherical parts:

$$\boldsymbol{\sigma}(t) = \boldsymbol{\sigma}'(t) + \frac{1}{3} \text{tr}(\boldsymbol{\sigma}(t)) \mathbf{I} \quad (8)$$

where  $\text{tr}(\boldsymbol{\sigma}(t))$  is the first stress invariant given by

$$\text{tr}(\boldsymbol{\sigma}(t)) = (\sigma_{xx}(t) + \sigma_{yy}(t) + \sigma_{zz}(t)) \quad (9)$$

The stress deviator  $\boldsymbol{\sigma}'(t)$  is computed as:

$$\boldsymbol{\sigma}'(t) = \begin{pmatrix} \frac{2\sigma_{xx} - \sigma_{yy} - \sigma_{zz}}{3} & \sigma_{xy} & \sigma_{xz} \\ \sigma_{yx} & \frac{2\sigma_{yy} - \sigma_{xx} - \sigma_{zz}}{3} & \sigma_{yz} \\ \sigma_{zx} & \sigma_{zy} & \frac{2\sigma_{zz} - \sigma_{xx} - \sigma_{yy}}{3} \end{pmatrix} \quad (10)$$

For a cyclic loading, the hydrostatic stress  $P_H(t)$  is a periodic scalar function. Its maximum value is:

$$P_{H, \max} = \frac{1}{3} \max\{\text{tr}(\boldsymbol{\sigma}(t))\} \quad (11)$$

For example, the maximum hydrostatic stress  $P_{H, \max}$  during a loading cycle of synchronous sinusoidal out-of-phase stresses Eq. 1 can be calculated analytically as:

$$P_{H, \max} = \frac{1}{3} \left[ \sqrt{\sigma_{x,a}^2 + \sigma_{y,a}^2 + 2\sigma_{x,a}\sigma_{y,a}\cos\beta} + (\sigma_{xm} + \sigma_{ym}) \right] \quad (12)$$

### 2. Transform the Stress Deviator $\boldsymbol{\sigma}'(t)$ to Reduced Euclidean Space

To make it easier to compute the shear stress amplitude, the following transformation rules can be used [6]:

$$S_1 = \frac{\sqrt{3}}{2} \sigma'_{xx}, \quad S_2 = \frac{1}{2} (\sigma'_{yy} - \sigma'_{zz}), \quad S_3 = \sigma'_{xy}, \quad S_4 = \sigma'_{xz}, \quad S_5 = \sigma'_{yz} \quad (13)$$

where  $\sigma'_{xx}, \sigma'_{yy}, \sigma'_{zz}, \sigma'_{xy}, \sigma'_{xz}, \sigma'_{yz}$  are the six components of the deviatoric stress vector  $\boldsymbol{\sigma}'(t)$ , and  $S_1, S_2, S_3, S_4, S_5$  are the five components of the transformed deviatoric stress vector  $\mathbf{S}(t)$ . With the above transformation, the deviatoric stress vector  $\boldsymbol{\sigma}'(t)$  is mapped onto a vector  $\mathbf{S}(t)$  in a 5-dimensional Euclidean space  $E_5$ . In this way, the stress deviator is fully described by a smaller number of components in the transformed space. During a periodic loading, the tip of the vector  $\mathbf{S}(t)$  describes a closed curve  $\Phi'$  in the transformed deviatoric stress space.

### 3. Computation of the Equivalent Shear Stress Amplitude

In the transformed deviatoric stress space, the loading path is a closed curve  $\Phi'$  in the deviatoric hyperplane. If the local stress-time histories are the synchronous sinusoidal waveforms as expressed in Eq. 1, the equivalent shear stress amplitude can be calculated directly using Eq. 2. When the local stress-time histories are irregular waveforms, a numerical approach with a sequential linear programming optimizer in conjunction with the simplex method can be employed to find the major semi-axis radius  $R_a$  and the minor semi-axis radius  $R_b$  of the minimum circumscribed ellipse. Then, the equivalent shear stress amplitude can be calculated as  $\tau_a = \sqrt{R_a^2 + R_b^2}$ .

### 4. Fatigue Life Prediction

Once the equivalent shear stress amplitude  $\tau_a$  and the maximum hydrostatic stresses  $P_{H,\max}$  throughout a general multiaxial loading block have been computed correctly following the above steps, the fatigue life  $N$  can be obtained from the iterative solution of the formulation of the Crossland's criterion ( or the Sines Criterion) by using the Newton-Raphson algorithm:

$$\tau_a + k(N)P_{H,\max} = \lambda(N) \quad (14)$$

where

$$k(N) = \left( \frac{3t_{-1}(N)}{f_{-1}(N)} \right) - \sqrt{3} \quad \lambda(N) = t_{-1}(N) \quad (15)$$

$f_{-1}(N)$  and  $t_{-1}(N)$  are the uniaxial reversed bending fatigue strength and the reversed torsion fatigue strength at  $N$  cycles, respectively.

## APPLICATION EXAMPLES AND VALIDATION OF THE PROPOSED APPROACH

Most of the published experimental results were obtained from the cylinder or bar specimens under Biaxial or Triaxial synchronous sinusoidal stresses as expressed in Eq. 1, so the closed form formulations of the general approach proposed in this paper can be applied easily for prediction. The verification of the proposed approach uses experimental data collected from the literature shows good correlation between predictions and experiments. Due to space limitation, only the comparison with Simburger's test results [16] is shown in Table1. The last column of Table 1 shows the error index of the prediction expressed as the relative difference between the left and right hand sides of Eq. 14.

A group of biaxial fatigue loading cases ( $\sigma_{xx}$  and  $\sigma_{yy}$ ) including the out-of-phase angles, different waveforms and different frequencies as shown in Fig. 3 is analyzed by the approach proposed and implemented in this paper. The loading path corresponding to each load case in the transformed deviatoric stress space is shown in Fig. 4. It may be noticed that the loading path curves are strongly influenced by the out-of-phase angles,

waveforms and frequency ratios. The last two rows in Table 2 display the shear stress amplitude values obtained with the definition used by the current approach (the minimum circumscribed circle approach) and the definition proposed in this paper, respectively. It is shown that the new approach can characterize the non-proportional loading effects. Table 3 shows the comparison between the predicted and the experimental result by McDiarmid [17]. Where  $\sigma_A$  is the uniaxial longitudinal fatigue strength at  $10^6$  cycles,  $\sigma_{1a}$  is the allowable maximum principal stress amplitude for each load case at  $10^6$  cycles.  $\sigma_{1a} / \sigma_A$  represents the reduction of fatigue strength due to the bi-axial loading effects. Agreement between predicted and experimental fatigue strength is satisfactory.

As an application example, fatigue analysis of a torque arm of an automotive rear suspension was carried out. As shown in Fig. 5, the model is fixed at the rim of the larger hole and loaded at the edge of the smaller hole with dynamic forces  $F_x(t)$  and  $F_y(t)$ . Quasi-static finite element analyses of this component were performed using unit load vectors using the ANSYS [18] finite element code. The stress influence coefficients obtained from these analyses were then superimposed with the dynamic loads  $F_x(t)$  and  $F_y(t)$  to compute dynamic stress histories at each node point of the component. Then, node fatigue damage evaluation was carried out as a post-processor with the procedures presented above. Fig. 6 shows the fatigue damage contour plot of the torque arm component.

## CONCLUSIONS

The minimum circumscribed ellipse approach provides an efficient and easy-to-use approach to fully characterize the non-proportional loading effects. With this new approach for evaluating the effective shear stress amplitude, the Sines and Crossland multiaxial fatigue criteria can be extended for finite fatigue life prediction. Multiaxial fatigue test results collected from the literature, including complex stress histories with different waveforms, frequencies, out-of-phase angles and mean stresses, are used for validating the developed approach in this paper. The correlation is satisfactory. The numerical algorithm for computation of the major and minor ellipse semi-axes, required to evaluate the shear stress amplitude and mean value, is general and efficient. It provides an unified approach for fatigue design, that is particularly suitable for integration with computer aided design.

## REFERENCES

1. Bannantine, J.A. and Socie, D.F. (1991) *ESIS10*, Kussmaul, K., McDiarmid, D., Socie, D. Eds, pp. 35-51.
2. Dang-Van, K. (1993) in *ASTM STP 1191*, D.L. McDowell and R. Ellis. Eds., pp. 120-130.
3. Wang, C.H. and Brown, M.W. (1996) *ASME J. Engng. Mater. Technology* **118**, 367.
4. Robert, J.L., Fogue, M. and Bahuaud, J., (1994) in *ASTM STP 1231*, C. Amzallag, Ed., pp.369-387.
5. Liu Jiping (1997) *Proceed. 5th Int. Conf. Biaxial/Multiaxial Fatigue & Fracture*, Poland, pp.45-62.
6. Papadopoulos, I.V.(1997) *Advanced Course on High-cycle Metal Fatigue*, CISM, Udine, Italy.
7. McDowell, D.L. (1996) *International Journal of Fracture* **80**, pp.103-145.
8. Sines, G., (1959) *Metal Fatigue*, McGraw Hill, New York, pp.145-169.
9. Crossland, B., (1956) *Proc. Int. Conf. on Fatigue of Metals*, London, pp.138-149.
10. Fuchs, H.O. and Stephens, R.I., (1980) *Metal Fatigue in Engineering*, Addison-Wesley.
11. Heidenreich, R., Zenner H. and Richter I., (1983) *Forschungshefte FKM*, Heft 105.
12. Li, B., (1999) Ph.D. thesis, Technical University of Lisbon, Portugal.
13. Li, B., Santos, J.L.T.and de Freitas, M., (2000) *Mechanics of Structures and Machines*, **28**, pp.85-103.
14. Freitas, M., Li, B. and Santos, J.L.T., to appear in *ASTM STP 1387*.
15. Arora, J.S., (1989) *Introduction to Optimum Design*, McGraw-Hill, New York.
16. Simburger, A., (1975) LBF Darmstadt, Bericht, Nr-FB-121.
17. McDiarmid, D.L., (1989) *Biaxial and Multiaxial Fatigue*, EGF3 Mech. Eng. Pub., London, pp.557-573.
18. ANSYS 5.0 (1992) Swanson Analysis Systems, Inc., Houston, PA 15342-0065.

TABLE 1: Comparison with Simburger's tests [16], Material=CK45  
 $N=100\,000$  cycles,  $f_1(N) = 423$  MPa,  $t_1(N) = 287$  MPa

Stresses [MPa] expressed in Eq. 1								Error Index
$\sigma_{x,a}$	$\sigma_{x,m}$	$\sigma_{y,a}$	$\sigma_{y,m}$	$\sigma_{xy,a}$	$\sigma_{xy,m}$	$\beta$	$\gamma$	I (%)
234	0	256	256	0	0	180	...	-4.81
300	-300	330	330	0	0	0	...	-13.16
275	-275	302	302	0	0	90	...	0.56
183	183	367	367	0	0	0	...	2.69
250	250	275	275	0	0	180	...	10.87
327	0	0	0	188	0	...	0	4.35
250	250	0	0	144	0	...	90	-11.34
288	0	0	0	165	165	...	90	-8.23
292	0	0	0	167	0	...	60	-7.03
285	0	0	0	163	163	...	0	-9.26
304	0	0	0	174	0	...	90	-3.18

TABLE 2: Comparison between results by the new approach (Minimum Circumscribed Ellipse) and the current approach (Minimum Circumscribed Circle)

	case 1	case 2	case 3	case 4	case 5	case 6
Major semi-axis $R_a$	188.2	256.5	326.0	306.2	188.0	326.0
Minor semi-axis $R_b$	0	233.1	148.0	177.0	187.0	188.0
$\tau_a$ (Current approach), MPa	188.2	256.5	326.0	306.2	188.0	326.0
$\tau_a$ (New approach), MPa	188.2	346.6	358.0	353.6	265.4	376.5

TABLE 3: Comparison between predicted and experimental fatigue strength results [17]

Load Case	$\sigma_{1a}/\sigma_A$ (predicted)	$\sigma_{1a}/\sigma_A$ (experiment)
1	0.81	0.82
2	0.57	0.63
3	0.58	0.57
4	0.56	0.63

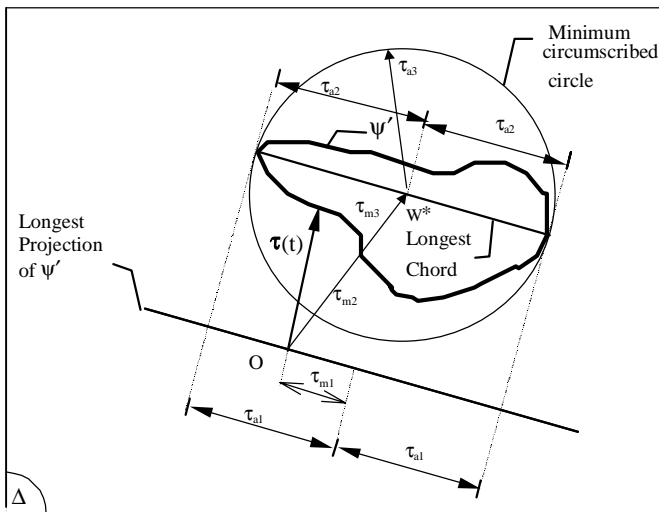


Figure 1: The current approaches for evaluating the amplitude and mean value of shear stresses  $\tau(t)$ .

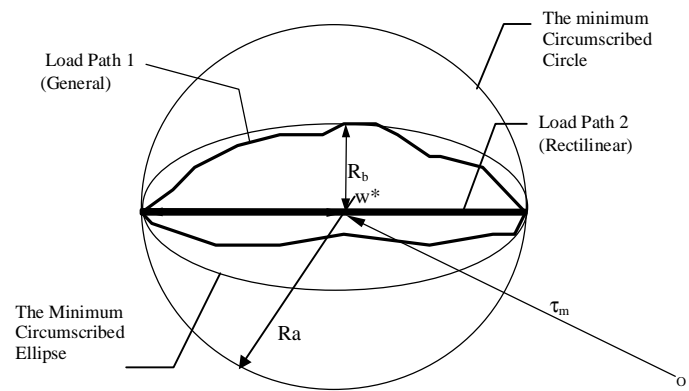
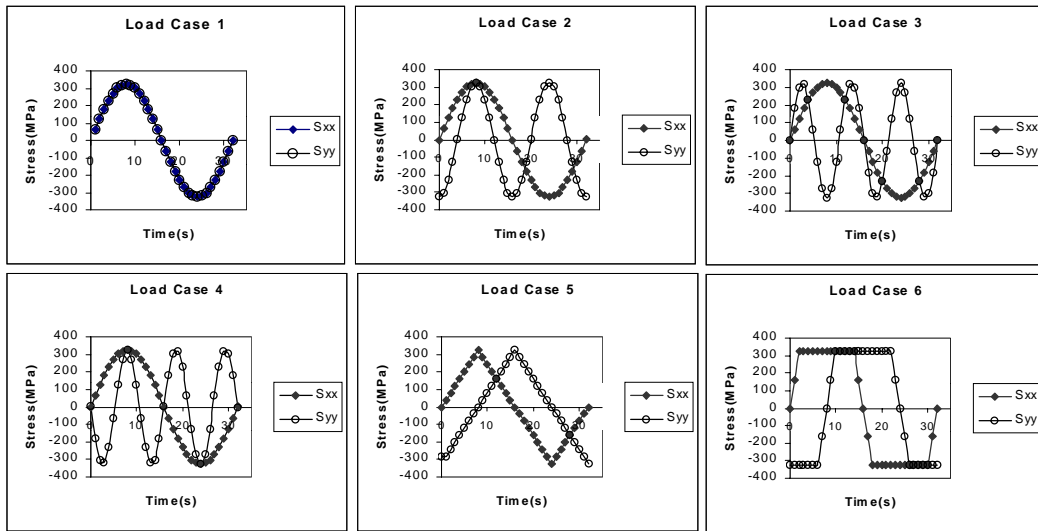
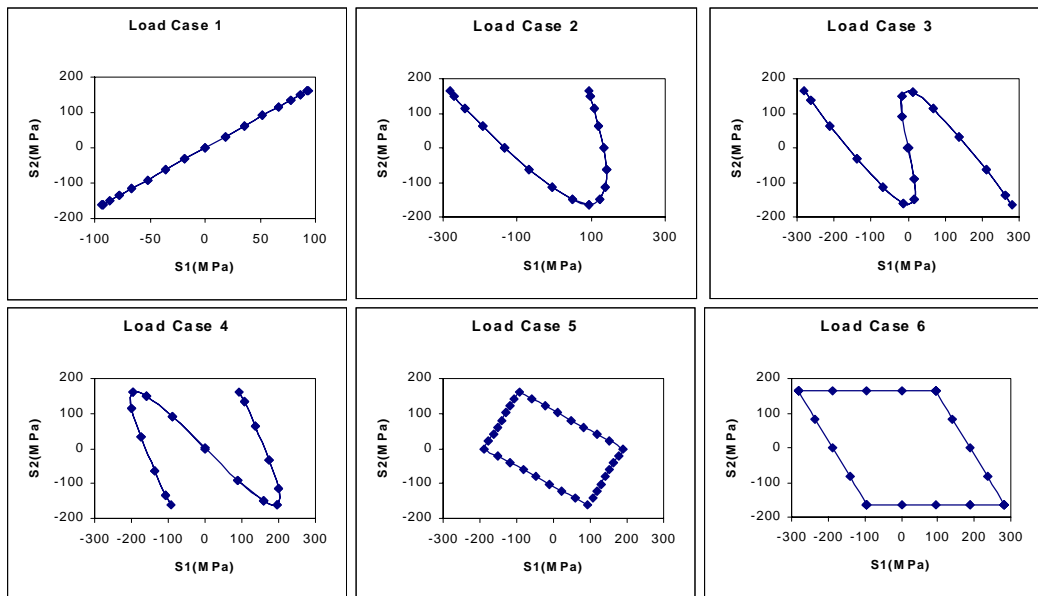


Figure 2: The minimum circumscribed circle and ellipse approaches.



**Figure 3:** Biaxial stress histories of load case 1—6.



**Figure 4:** The loading paths of load case 1-6 in the transformed deviatoric stress space.

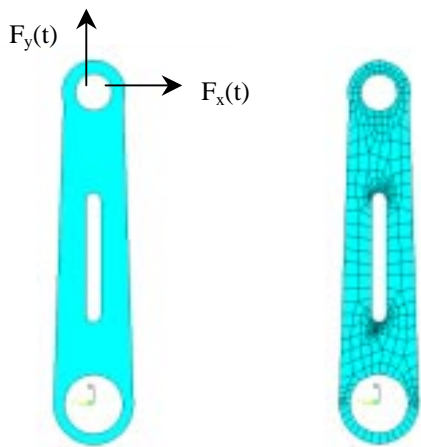


**Figure 5:** The example torque arm model and meshes.

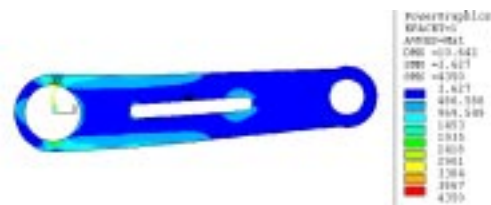


**Figure 6:** Fatigue damage contour plot.